PHYSICAL REVIEW A VOLUME 36, NUMBER 5 SEPTEMBER 1, 1987

Neutron diffraction on subcritical and supercritical krypton

Henk Fredrikze
Interuniversitair Reactor Instituut, Mekelweg 15, NL-2629JB Delft, The Netherlands
(Received 5 January 1987)

Accurate neutron-diffraction data are presented for krypton at three densities along a supercritical ($T=220$ K) isotherm and at three densities in the liquid state along a subcritical ($T=200$ K) isotherm. The density dependence of the Fourier transform of the total correlation function, $H(\kappa)$, differs significantly from the one for dense liquid rare gases determined from recent neutron scattering data. Comparisons with modified-hypernetted-chain and molecular-dynamics calculations suggest that the present data cannot be described adequately with a reliable pair potential and an (effective) Axilrod-Teller three-body potential.

I. INTRODUCTION

Egelstaff and co-workers[1,2] concluded from neutron-diffraction data on gaseous krypton at low (subcritical) densities and room temperature that the structure of these systems cannot be described adequately with a reliable two-body potential (e.g., taken from either Barker *et al.*[3] or Aziz and Slaman[4]) together with a first-order Axilrod-Teller (AT) triple-dipole three-body correction.[5] In contrast Aers and Dharma-wardana[6] showed that the data could be described satisfactorily using the Barker pair potential in combination with an effective AT three-body contribution in the modified-hypernetted-chain (MHNC) approximation. Schommers[7] obtained a quantitative agreement between the experimental data and molecular-dynamics (MD) calculations with the Barker potential together with AT.

Recently Barker[8] reconfirmed that more-body interactions largely cancel to yield effectively AT as the only more-body interaction for the quantitative description of thermodynamic properties in rare-gas systems. At the same time he discussed the disagreement between the data of Egelstaff *et al.*[1] and the effective AT model, and advised that "... these neutron-scattering results must be treated with reserve." On the other hand, according to Egelstaff[9] AT as the only (effective) more-body interaction is also in conflict with measurements of the dynamic structure factor[10] compared with computer simulations.[2,11–13] His conclusion is that structure and dynamics of a fluid system may depend more sensitively on the details of the more-body interaction potential than thermodynamic quantities, which are represented by integrals of the potential.

In view of the lack of consensus on the role of the AT three-body potential as an effective more-body potential, more experimental (and simulation) data on the structure (and dynamics) of noble-gas systems are needed. In this connection it is appropriate to report on recent accurate neutron-diffraction experiments on krypton at three densities along a supercritical isotherm $T=220$ K ($T_c=209$ K) and at three densities along a subcritical isotherm $T=200$ K (in the liquid phase). In this paper the relation between neutron-diffraction data and the microscopic structure of a monatomic fluid is briefly introduced (avoiding the confusing and unjustified concept of incoherent scattering[14]), followed by a short description of the diffractometer and the experiments. Then the various corrections are discussed that were applied to the experimental data to extract the structure factor.

The corrected data are presented and the nontrivial part of the density dependence of the structural data is compared with results from recent experiments on noble-gas systems. The data are compared with MHNC calculations with the Barker pair potential with and without a lowest-order effective AT correction. In contrast to the data on gaseous krypton at room temperature, no satisfactory agreement could be obtained with the present data. The same conclusion is reached from comparison with MD simulations by Barocchi *et al.*[15] In the r range relevant to the structure of fluid krypton, the pair potentials of Barker[3] and of Aziz[4] are practically identical, as is confirmed by MHNC calculations; therefore, it may be expected that a comparison between the experimental data and theoretical predictions does not depend on the choice between these two pair potentials.

II. NEUTRON DIFFRACTION ON MONATOMIC FLUIDS

In neutron diffraction experiments the intensity of neutrons scattered by a sample from a monochromatic beam is measured as a function of the scattering angle θ. A neutron with mass m_n, wave vector $\mathbf{k}_0$ before and $\mathbf{k}$ after scattering, has suffered a momentum transfer

$$\hbar\boldsymbol{\kappa}=\hbar(\mathbf{k}_0-\mathbf{k}) \tag{1}$$

and an energy transfer

$$\hbar\omega=\frac{\hbar^2(\mathbf{k}_0^2-\mathbf{k}^2)}{2m_n} . \tag{2}$$

The intensity $I(\theta,\omega)$ at an angle θ with the incoming beam per unit of ω is proportional to the detector efficiency $\epsilon(k)$ and the double differential scattering cross section $d^2\sigma/d\Omega\, d\omega$,[16] which in the first Born approximation may be separated into a self part and a distinct part

$$\frac{d^2\sigma}{d\Omega\, d\omega}=\frac{k}{k_0}[S_s(\boldsymbol{\kappa},\omega)+S_d(\boldsymbol{\kappa},\omega)] ,$$

$$S_s(\boldsymbol{\kappa},\omega)=\frac{1}{2\pi N}\sum_i \langle b_i b_i^* \rangle \int_{-\infty}^{\infty} \exp(-i\omega t)\langle \exp(-i\boldsymbol{\kappa}\cdot\mathbf{r}_i)\exp[i\boldsymbol{\kappa}\cdot\mathbf{r}_i(t)]\rangle dt , \tag{3}$$

$$S_d(\boldsymbol{\kappa},\omega)=\frac{1}{2\pi N}\sum_{i\neq j} \langle b_i \rangle \langle b_j^* \rangle \int_{-\infty}^{\infty} \exp(-i\omega t)\langle \exp(-i\boldsymbol{\kappa}\cdot\mathbf{r}_i)\exp[i\boldsymbol{\kappa}\cdot\mathbf{r}_j(t)]\rangle dt .$$

The summations are over all atoms in the sample. The angle brackets around the exponentials that depend on the positions $\mathbf{r}_j(t)$ of the atoms at time t (omitted for $t=0$) indicate a thermal average which in general depends on the mass of the atoms. The brackets around the scattering lengths b_j, which depend on the spin state of the atom and the type of isotope (b_j is complex if absorption plays a role[17]), indicate an average over the spin states only. The inextricable coupling of the mass and the scattering length for a particular atom forbids one to replace at this stage the average over the spin states by an average also over the isotopic distribution for an isotopic monatomic mixture.[14] For isotropic homogeneous fluids the dynamical scattering function depends on $\boldsymbol{\kappa}$ only through the modulus $\kappa=|\boldsymbol{\kappa}|$ and the notation $S(\kappa,\omega)$ is used.

The intensity in diffraction experiments is the integral of $I(\theta,\omega)$ over ω,

$$I(\theta)\sim \int_\theta \frac{k}{k_0}\epsilon(k)[S_s(\kappa,\omega)+S_d(\kappa,\omega)]d\omega . \tag{4}$$

At constant scattering angle κ and ω are not independent and $I(\theta)$ may be expanded (Yarnell *et al.*[18]) in the moments (and their κ derivatives) of the dynamical scattering functions $S(\kappa,\omega)$,

$$\hbar^n\langle\omega^n\rangle=\hbar^n\int_{-\infty}^{\infty}\omega^n S(\kappa,\omega)d\omega . \tag{5}$$

For an isotopic mixture of a monatomic fluid the lower moments are[14]

$$\begin{aligned}
&\langle\omega^0\rangle_s=\langle b^2\rangle ,\\
&\langle\omega^0\rangle_d=\langle b\rangle^2\frac{1}{N}\sum_{\substack{i,j\\(i\neq j)}}\langle\exp(-i\boldsymbol{\kappa}\cdot\mathbf{r}_i)\exp(i\boldsymbol{\kappa}\cdot\mathbf{r}_j)\rangle ,\\
&\hbar\langle\omega\rangle_s=\frac{1}{2}\left\langle\frac{b^2}{m}\right\rangle\hbar^2\kappa^2 ,\\
&\hbar\langle\omega\rangle_d=0 .
\end{aligned} \tag{6}$$

The angle brackets around the scattering lengths here denote the average over both the spin states and the isotopic distribution of the sample atoms and $\kappa=2k_0\sin(\frac{1}{2}\theta)$ is the elastic value of the scattering parameter. To lowest order

$$I(\kappa)\sim\epsilon(k_0)\Delta\Omega\{\langle b^2\rangle+\langle b\rangle^2[S(\kappa)-1]\} , \tag{7}$$

where the structure factor $S(\kappa)$ (in the classical approximation) is given by

$$S(\kappa)=\frac{1}{N}\sum_{i,j}\langle\exp(-i\boldsymbol{\kappa}\cdot\mathbf{r}_i-\mathbf{r}_j)\rangle . \tag{8}$$

Introduction of the reduced generic two-particle distribution function or pair correlation function[19] $g_2(\mathbf{r},\mathbf{r}')$ leads to

$$S(\kappa)=1+\frac{n^2}{N}\int\int g_2(\mathbf{r},\mathbf{r}')\exp(-i\boldsymbol{\kappa}\cdot\mathbf{r}-\mathbf{r}')d\mathbf{r}\,d\mathbf{r}' . \tag{9}$$

with n the number density. Except in the region of extremely small κ values $S(\kappa)$ can be approximated by[20]

$$S(\kappa)=1+n\int[g(r)-1]\exp(-i\boldsymbol{\kappa}\cdot\mathbf{r})d\mathbf{r} , \tag{10}$$

where $g(r)=g_2(\mathbf{r}',\mathbf{r}'')$ with $r=|\mathbf{r}'-\mathbf{r}''|$. The isotropy of the scattering system leads to the well-known Zernike-Prins relations,[21] here written as

$$\begin{aligned}
&H(\kappa)=\frac{S(\kappa)-1}{n}=\frac{4\pi}{\kappa}\int_0^\infty rh(r)\sin(\kappa r)dr ,\\
&h(r)=\frac{1}{2\pi^2 r}\int_0^\infty \kappa H(\kappa)\sin(\kappa r)d\kappa ,
\end{aligned} \tag{11}$$

with $h(r)=g(r)-1$ the total correlation function.[22] Obviously $S(\kappa)$ is the proper quantity to describe a scattering pattern; however, $H(\kappa)$ should be considered if information on $h(r)$ is to be extracted from the data. Therefore $H(\kappa)$ and its density dependence will be discussed rather than $S(\kappa)$.

It can be shown[21] that, as long as Eq. (10) is a valid approximation,[20] the low-κ limit for $S(\kappa)$ is related to the isothermal compressibility χ_T,

$$S(0)=\lim_{\kappa\to 0}S(\kappa)=nk_B T\chi_T , \tag{12}$$

or, equivalently,

$$H(0)=\lim_{\kappa\to 0}H(\kappa)=k_B T\chi_T-\frac{1}{n} . \tag{13}$$

III. THE DIFFRACTOMETER

For the experiments the diffractometer at the 2-MW swimming-pool reactor of Interuniversitair Reactor Instituut (IRI) Delft was used. This is a conventional two-axis diffractometer with a single detector.[17] The wavelength of the "monochromatic" beam, $\lambda=0.0881$ nm, reflected from the 002 lattice planes of the Zn monochromator, with mosaic spread of 20′ full width at half maximum (FWHM), was determined experimentally from diffraction on powdered Ni and KI. The contribution of higher-order wavelengths was determined to be less than 1% from transmission experiments on thin Cd sheets. The beam path from the reactor core to the sample was evacuated. The cross section of the mono-

chromatic beam, with a divergence of 42′ FWHM, was 2.25×7.0 cm^2 at the sample position. A low-efficiency ($\approx10^{-4}$) fission chamber was placed in the beam to monitor the flux on the sample. Intensities were measured at equidistant values of the scattering parameter κ with a 2-inch ^{3}He detector with high efficiency ($\approx97\%$ at $\lambda=0.09$ nm) 56 cm from the sample. To reduce the background a Cd mask of 2.25×7.0 cm^2 was mounted on the detector arm close to the cryostat with the sample. Another Cd mask of 2.0×5.0 cm^2 was mounted in front of the detector collimator, which had a divergence of 42′ FWHM. The maximum scattering angle $\theta=130°$ corresponds to $\kappa=129$ nm^{-1}. It is not expected that effects of instrumental resolution will be significant on the relatively broad and smooth features of the intensity patterns (cf. Ref. 23) and no attempts were made to correct the experimental data for the finite resolution.

The operation of the diffractometer, connected to the central Digital Equipment Corporation PDP11/70 computer via CAMAC (computer-aided measurement and control standard), was controlled by a program that started automatically whenever the computer was restarted. The data collection, in the preset monitor mode, continued as soon as the monitor count rate exceeded a minimum value; thus data were taken whenever the computer and the reactor were active simultaneously. A measurement of the intensity at each detector position was divided into ten submeasurements, which were checked on line on statistical consistency before the average was accepted as a data point. This test of the short term stability is described in detail in Appendix A.

IV. THE EXPERIMENTS

The samples were kept in a circular cylindrical container (height 72 mm, wall thickness 0.4 mm, and diameter 20 mm) manufactured from V sheet by electron-beam welding. The bottom and the top flange, fabricated from a special Ni-Fe (45%-55%) alloy, were fitted to the cylinder using high-temperature soldering technique. The top flange was sealed leak tight, with screws and a metal *O* ring, to a lid of the Ni-Fe alloy.

The lid was attached to the bottom of the N_2 vessel of a bath cryostat, with Al walls 20 cm in diameter, via a brass block kept at a constant temperature by a control unit (Oxford Instruments). The container was surrounded by a wide Al radiation shield (19 cm diameter) such that neutrons scattered from the shield could not enter the detector. The temperature of the top flange, measured continuously with a calibrated precision Pt-resistance thermometer (Rosemount), was constant within 0.05 K.

The 99.995% pure krypton was filled into the container through a stainless-steel capillary that connected the container with a gas-handling system that consisted of a small cryo vessel (30 cm^3), the storage bottle, a safety valve, and a pressure transducer (Druck, PDRC-32). The sample was connected to the safety valve continuously and to the pressure transducer only periodically to check the pressure, which varied less than 15 kPa at each thermodynamic state.

The samples were measured at three densities

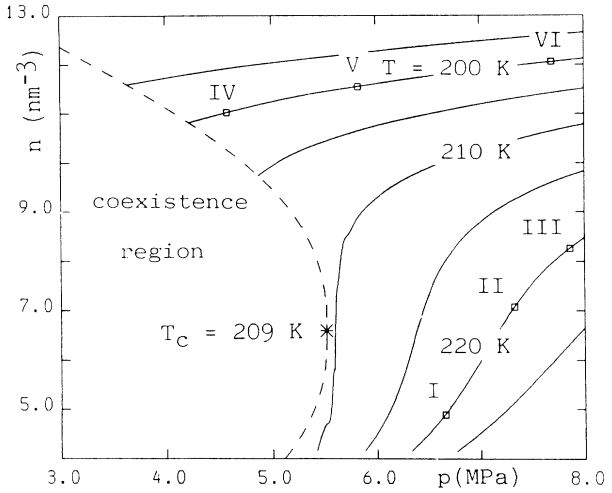

FIG. 1. Number density as a function of pressure for krypton. The thermodynamic states of the experiments along the supercritical 220-K and subcritical 200-K isotherms are indicated.

($n=4.89$, 7.08, and 8.26 nm^{-3}) along the 220-K isotherm in the gas phase, and at three densities ($n=11.02$, 11.55, and 12.06 nm^{-3}) along the 200-K isotherm in the liquid phase. The densities were calculated from *p-V-T* data of Theeuwes and Bearman.[24] The thermodynamic states are plotted in Fig. 1, together with the critical point.

Below $\kappa=4$ nm^{-1} the background was extremely high and data were taken only in the range $4\leq\kappa\leq129$ nm^{-1} in steps of 0.5 nm^{-1} in repeated series for the samples, the empty container, the background, and a Cd bar of the same size as the container. The number of series was optimized such that after correction for background and container scattering the experimental structure factors $S(\kappa)$ each would have the same statistical accuracy ($\approx0.3\%$). The requirement that this should be the best statistical accuracy obtainable in the time totally spent on the measurements, determines the apportionment of time (i.e., the number of repeated series for each sample condition). The number of series, each with a duration of approximately one day, was 2 for the background, 31 for the

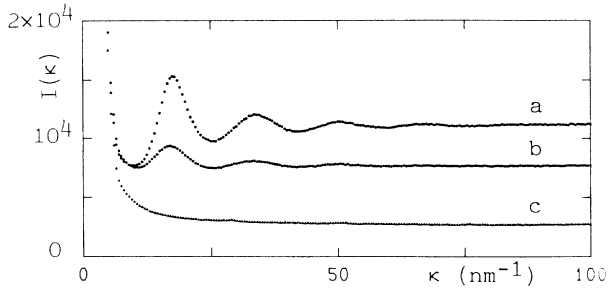

FIG. 2. Uncorrected intensities normalized to 10^5 monitor counts. (a) The krypton sample at the higher density in the liquid phase, (b) the same at the lower density in the gaseous phase, (c) the empty container.

empty container; 38, 35, and 33 for the three gas samples at $T=220$ K; and 23, 24, and 19 for the liquid samples at $T=200$ K. At low κ values, up to 30 nm^{-1}, additional measurements were done with the empty beam, the empty container, and the Cd bar. The repeated series of measurements were checked on statistical consistency and averaged off line. (Cf. Appendix A for details on the statistical checks.) In Fig. 2 the intensities are shown for the container, the gaseous sample at the lower density, and the liquid sample at the higher density.

V. BACKGROUND AND MULTIPLE SCATTERING

The background $I_0(\kappa)$, measured with the container removed, can be separated into a part that is attenuated by scattering and absorption in the container and/or sample, and an unattenuated part. The latter $I_{Cd}(\kappa)$, measured separately with a Cd bar of exactly the same outer dimensions as the container, must be subtracted without any correction factor from all measurements. The difference between $I_0(\kappa)$ and $I_{Cd}(\kappa)$, due to neutrons that pass the sample position, should be subtracted multiplied by T_s, the transmission of the sample and/or the container, calculated numerically. The correction for background then yields

$$I_s^*(\kappa)=I_s(\kappa)-I_{Cd}(\kappa)-T_s[I_0(\kappa)-I_{Cd}(\kappa)] . \tag{14}$$

The observed intensity is the sum of contributions $I_n(\kappa)$ of n-fold scattered neutrons

$$I(\kappa)=\sum_{n=1}^{\infty} I_n(\kappa) . \tag{15}$$

The probability for a sequence of scattering points $\mathbf{r}_1, \ldots, \mathbf{r}_n$ depends on the microscopic scattering properties

$$P(\mathbf{r}_1,\mathbf{r}_2, \ldots, \mathbf{r}_n)\sim\Phi(\mathbf{r}_1)\prod_{i=1}^{n}\mu_{scat}(\mathbf{r}_i)S(\kappa_i;\mathbf{r}_i) , \tag{16}$$

with $\mu_{scat}(\mathbf{r}_i)$ the linear scattering coefficient in the sample or, depending on $\mathbf{r}_i$, the container and similarly for $S(\kappa_i;\mathbf{r}_i)$. $\Phi(\mathbf{r}_1)$ represents the relative incoming flux. The attenuation along a path for n-fold scattering is $\exp(-\Sigma_n)$ with Σ_n the integral of the linear attenuation coefficient along that path. Integration over the volume of sample and container yields

$$I_n(\kappa)\sim\frac{1}{(4\pi)^{n-1}}\int\int\cdots\int\frac{P(\mathbf{r}_1,\mathbf{r}_2, \ldots, \mathbf{r}_n)\exp(-\Sigma_n)}{|\mathbf{r}_2-\mathbf{r}_1|^2\,|\mathbf{r}_3-\mathbf{r}_2|^2\cdots|\mathbf{r}_n-\mathbf{r}_{n-1}|^2}d\mathbf{r}_1\,d\mathbf{r}_2\cdots d\mathbf{r}_n . \tag{17}$$

$\Phi(\mathbf{r}_1)$ restricts the integration of the first scattering point to the illuminated part of the sample or the container. The sum of $I_n(\kappa)$ for $n\geq 2$ is called multiple scattering,

$$I_{mult}(\kappa)=\sum_{n=2}^{\infty} I_n(\kappa) . \tag{18}$$

$I_n(\kappa)$ depends implicitly on $S(\kappa)$. Vineyard[25] assumed that the multiple scattering is independent of the structure factor (the quasi-isotropic approximation)

$$\begin{aligned} I_{mult}(\kappa)&\approx I_1'(\kappa)\sum_{k=2}^{\infty}\prod_{n=2}^{k}\delta_n(\kappa) , \\ \delta_n(\kappa)&=\frac{I_n'(\kappa)}{I_{n-1}'(\kappa)}, \quad (n\geq 2) . \end{aligned} \tag{19}$$

The prime denotes intensities in the quasi-isotropic approximation. $I_n'(\kappa)$ cannot be calculated straightforwardly for arbitrary values of n because of the many integrations and often only $\delta_2(\kappa)$ for a bare sample is calculated while $\delta_n(\kappa)$ is estimated from $\delta_2(\kappa)$. Vineyard[25] proposed the approximation

$$\delta_n\approx\delta_2 \quad (n>2) . \tag{20}$$

In the present experiments the samples scattered 8–12%. The container, which scattered approximately 4%, caused a non-negligible contribution to the multiple scattering. Therefore the multiple scattering was estimated with the code MSCAT,[26–28] which simulates neutron histories by Monte Carlo techniques. In the quasi-isotropic approximation $\Delta(\kappa)$, the ratio of multiple scattering and total scattering (omitting the primes),

$$\Delta(\kappa)=\frac{I_{mult}(\kappa)}{I_{1,s}(\kappa)+I_{1,c}(\kappa)+I_{mult}(\kappa)} , \tag{21}$$

is a useful quantity. As a function of the density of the krypton $\Delta(\kappa)$ is shown in Fig. 3 for the sample in the container and for the bare sample, together with results of a straightforward calculation using the Vineyard approxi-

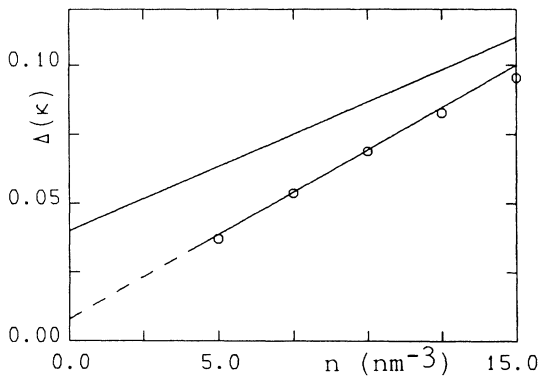

FIG. 3. $\Delta(\kappa)$ as a function of the density of the krypton sample in the container (upper line) and for the bare sample (lower line). Circles are from straightforward calculation and Vineyard's approximation.

mation Eq. (20). Clearly the influence of the container scattering cannot be ignored. Recently MSCAT was updated[29] and now also elastic scattering with specified $S(\kappa)$'s for the sample and the container can be simulated. For $S(\kappa)$'s that are not too pronounced, it turns out that the multiple scattering calculated with the two versions is not significantly different.

VI. ATTENUATION EFFECTS

The single scattering is the sum of sample scattering and container scattering,

$$\begin{aligned} I_1(\kappa) &\sim p_s(\theta)S_s(\kappa)+p_c(\theta)S_c(\kappa) , \\ p_s(\theta) &= \mu_s \int_{V_s} \Phi(\mathbf{r})\exp[-\Sigma_1(\mathbf{r};\theta)]d\mathbf{r} , \\ p_c(\theta) &= \mu_c \int_{V_c} \Phi(\mathbf{r})\exp[-\Sigma_1(\mathbf{r};\theta)]d\mathbf{r} , \end{aligned} \tag{22}$$

with μ_s and μ_c the linear scattering coefficients, $S_s(\kappa)$ and $S_c(\kappa)$ the structure factors, and V_s and V_c the volumes of the sample and the container. $\Sigma_1(\mathbf{r};\theta)$ is the integral of the linear attenuation coefficient along the particular path followed by a neutron scattered only once in the sample or the container in the direction θ. For completely illuminated cylindrical samples in a uniform beam the three-dimensional integrals reduce to two-dimensional integrals, that must be calculated numerically. The circular cylindrical symmetry is broken by the incoming beam, which results in an angular dependence of $p(\theta)$ also for circular cylindrical samples. The single scattering from the empty container,

$$I_1'(\kappa) \sim p_c'(\theta)S_c(\kappa) , \tag{23}$$

differs from the single scattering from the container with the sample present. The latter is obtained from $I_1'(\kappa)$ taking into account the attenuation factor $W(\kappa)$, defined as the ratio of $p_c(\theta)$ and $p_c'(\theta)$. The single scattering from the sample is then obtained from

$$I_s(\kappa) = I_1(\kappa) - W(\kappa)I_1'(\kappa) . \tag{24}$$

For a thin-walled circular cylindrical container in a uniform beam (wall thickness d of the container small compared to the radius R, and the product of the linear attenuation coefficient of the container material and wall thickness small compared to 1) $W(\kappa)$ can be approximated by

$$\begin{aligned} W(\kappa) \approx \frac{1}{2}\frac{\theta}{\pi} &+ \frac{1}{\pi}\int_0^{\theta/2} \exp[-4\mu R\cos(\alpha-\tfrac{1}{2}\theta)\sin\tfrac{1}{2}\theta]d\alpha \\ &+ \frac{1}{\pi}\int_0^{\pi} \exp(-2\mu R\sin\alpha)d\alpha , \end{aligned} \tag{25}$$

with μ the linear attenuation coefficient for the sample. The thin-wall limit for $W(\kappa)$ has been obtained earlier by Boutron and Mériel,[30] but seems not to have been used frequently in the literature on neutron scattering. Several analytical results can be obtained from $W(\kappa)$ in the thin-wall limit, e.g., in the forward and backward direction,[20]

$$\begin{aligned} W(\kappa=0) &\approx 1-\frac{4}{\pi}\mu R+(\mu R)^2-\frac{16}{9\pi}(\mu R)^3 , \\ W(\kappa=2k_0) &\approx 1-\frac{4}{\pi}\mu R+2(\mu R)^2-\frac{64}{9\pi}(\mu R)^3 . \end{aligned} \tag{26}$$

Note the difference with the expression for the transmission of a cylindrical sample,[20]

$$T \approx 1-\frac{\pi}{2}\mu R+\frac{4}{3}(\mu R)^2-\frac{\pi}{4}(\mu R)^3+\frac{64}{45}(\mu R)^4 . \tag{27}$$

Numerically calculated $W(\kappa)$'s for the present experiments could be represented excellently by a quadratic function in κ^2,

$$W(\kappa) = W(0)(1+a\kappa^2+b\kappa^4) . \tag{28}$$

The angular-dependent attenuation of the single scattering $I_s(\kappa)$ from the sample was taken into account by multiplication by the factor $1/V(\kappa)$,

$$I_s'(\kappa) = \frac{I_s(\kappa)}{V(\kappa)} , \tag{29}$$

where $V(\kappa)$, the ratio of $p_s(\theta)$ and $p_s(\theta=0)$, was calculated numerically.

Unlike the closely related first-order transmission factor for a (bare) cylindrical sample (cf. Sears[31,32]), $V(\kappa)$ for the samples in the container could not be represented with high accuracy by a linear function in κ^2, but a perfect fit could be obtained with a quadratic function in κ^2,

$$V(\kappa) = 1+c\kappa^2+d\kappa^4 . \tag{30}$$

VII. INELASTICITY AND NORMALIZATION

Expression (7) for the single scattering should be modified to include the effect of inelastic scattering,

$$I(\kappa) \sim \epsilon(k_0)\{\langle b^2\rangle + \langle b\rangle^2[S(\kappa)-1]+P(\kappa)\} , \tag{31}$$

where $P(\kappa)$ is called the Placzek or inelasticity correction. $P(\kappa)$ may be estimated from the (truncated) moment expansion according to Yarnell *et al.*[18] Unfortunately, the higher moments are not known exactly and in practice they are approximated by the corresponding moments for the perfect gas. The advantage of the Yarnell procedure is that it leads to the expansion (31). An alternative to this expansion is to estimate $P(\kappa)$ from numerical integration at constant scattering angle θ of reliable models for $S(\kappa,\omega)$ which fulfill properly the detailed balance condition[16]

$$S(\kappa,-\omega) = \exp(-\beta\hbar\omega)S(\kappa,\omega) . \tag{32}$$

The numerical-integration procedure introduces errors only because the model for $S(\kappa,\omega)$ is not exact, but in contrast to the Yarnell procedure no additional errors arise from truncation. Here the numerical-integration procedure with $S(\kappa,\omega)$ for a perfect gas, including properly the detailed balance condition, was used. Due to the large mass of krypton ($M \approx 85$) this leads to modest values of $P(\kappa)$ ($\approx 0.03\langle b^2\rangle$ at $\kappa = 129$ nm^{-1}).

The corrected data were assumed to be described by

TABLE I. $H(\kappa)$ (nm^3) for the states I–VI defined in Table II.

κ (nm^{-1})	I	II	III	IV	V	VI
4.0	-0.6459(134)	-0.4440(80)	-0.3388(77)	0.3835(47)	0.2922(47)	0.3071(37)
4.5	-0.0906(25)	-0.0648(15)	-0.0655(12)	-0.0239(9)	-0.0292(8)	-0.0234(8)
5.0	-0.0979(18)	-0.0750(12)	-0.0766(10)	-0.0485(6)	-0.0490(5)	-0.0461(5)
5.5	-0.0916(14)	-0.0777(8)	-0.0735(7)	-0.0436(5)	-0.0449(4)	-0.0445(4)
6.0	-0.0960(12)	-0.0821(7)	-0.0746(6)	-0.0550(4)	-0.0539(4)	-0.0540(4)
6.5	-0.0986(11)	-0.0817(6)	-0.0739(5)	-0.0533(4)	-0.0531(3)	-0.0532(3)
7.0	-0.0990(10)	-0.0833(6)	-0.0749(5)	-0.0541(3)	-0.0535(3)	-0.0532(3)
7.5	-0.0993(10)	-0.0821(6)	-0.0739(4)	-0.0550(3)	-0.0545(3)	-0.0536(3)
8.0	-0.0969(9)	-0.0804(5)	-0.0724(4)	-0.0557(3)	-0.0546(3)	-0.0548(3)
8.5	-0.0948(9)	-0.0786(5)	-0.0707(4)	-0.0558(3)	-0.0546(3)	-0.0536(3)
9.0	-0.0938(9)	-0.0767(5)	-0.0699(4)	-0.0559(3)	-0.0551(3)	-0.0551(3)
9.5	-0.0874(9)	-0.0742(5)	-0.0663(4)	-0.0552(3)	-0.0545(3)	-0.0538(3)
10.0	-0.0849(9)	-0.0708(5)	-0.0651(4)	-0.0542(3)	-0.0534(3)	-0.0527(3)
10.5	-0.0767(9)	-0.0656(5)	-0.0604(4)	-0.0523(3)	-0.0512(3)	-0.0510(3)
11.0	-0.0698(9)	-0.0610(5)	-0.0559(4)	-0.0495(3)	-0.0491(3)	-0.0489(3)
11.5	-0.0618(9)	-0.0547(5)	-0.0505(4)	-0.0456(3)	-0.0452(3)	-0.0455(3)
12.0	-0.0526(9)	-0.0469(5)	-0.0442(4)	-0.0410(3)	-0.0410(3)	-0.0420(3)
12.5	-0.0425(9)	-0.0387(5)	-0.0368(4)	-0.0367(3)	-0.0360(3)	-0.0372(3)
13.0	-0.0265(9)	-0.0270(5)	-0.0272(4)	-0.0282(3)	-0.0285(3)	-0.0299(3)
13.5	-0.0146(9)	-0.0184(5)	-0.0180(4)	-0.0206(3)	-0.0216(3)	-0.0228(3)
14.0	-0.0028(9)	-0.0068(5)	-0.0089(4)	-0.0116(3)	-0.0132(3)	-0.0146(3)
14.5	0.0090(9)	0.0032(5)	0.0015(4)	-0.0018(3)	-0.0027(3)	-0.0041(3)
15.0	0.0242(9)	0.0148(5)	0.0125(4)	0.0091(3)	0.0073(3)	0.0063(3)
15.5	0.0321(9)	0.0255(5)	0.0214(4)	0.0194(4)	0.0180(3)	0.0170(3)
16.0	0.0428(9)	0.0362(5)	0.0312(5)	0.0307(4)	0.0294(3)	0.0285(3)
16.5	0.0493(10)	0.0421(5)	0.0379(5)	0.0390(4)	0.0374(4)	0.0371(4)
17.0	0.0529(9)	0.0455(6)	0.0406(5)	0.0439(4)	0.0424(3)	0.0423(4)
17.5	0.0504(9)	0.0459(6)	0.0426(5)	0.0462(4)	0.0445(4)	0.0445(4)
18.0	0.0506(9)	0.0445(5)	0.0421(5)	0.0455(4)	0.0450(3)	0.0447(4)
18.5	0.0461(9)	0.0412(5)	0.0381(5)	0.0416(4)	0.0408(4)	0.0414(4)
19.0	0.0398(9)	0.0354(5)	0.0320(4)	0.0354(4)	0.0339(3)	0.0348(4)
19.5	0.0326(9)	0.0293(5)	0.0262(4)	0.0282(4)	0.0272(3)	0.0280(3)
20.0	0.0237(9)	0.0210(5)	0.0193(4)	0.0211(4)	0.0211(3)	0.0212(3)
20.5	0.0166(8)	0.0147(5)	0.0126(4)	0.0137(3)	0.0132(3)	0.0132(3)
21.0	0.0094(8)	0.0070(5)	0.0065(4)	0.0073(3)	0.0063(3)	0.0059(3)
21.5	0.0033(8)	0.0022(5)	0.0008(4)	0.0026(3)	0.0006(3)	0.0016(3)
22.0	-0.0040(8)	-0.0033(5)	-0.0023(4)	-0.0037(3)	-0.0039(3)	-0.0036(3)
22.5	-0.0059(8)	-0.0064(5)	-0.0077(4)	-0.0069(3)	-0.0071(3)	-0.0079(3)
23.0	-0.0110(8)	-0.0099(5)	-0.0102(4)	-0.0095(3)	-0.0104(3)	-0.0105(3)
23.5	-0.0148(8)	-0.0133(5)	-0.0130(4)	-0.0130(3)	-0.0127(3)	-0.0130(3)
24.0	-0.0178(8)	-0.0160(5)	-0.0153(4)	-0.0149(3)	-0.0147(3)	-0.0147(3)
24.5	-0.0193(8)	-0.0177(5)	-0.0158(4)	-0.0159(3)	-0.0154(3)	-0.0155(3)
25.0	-0.0187(8)	-0.0166(5)	-0.0158(4)	-0.0160(3)	-0.0161(3)	-0.0166(3)
25.5	-0.0187(8)	-0.0174(5)	-0.0162(4)	-0.0159(3)	-0.0157(3)	-0.0165(3)
26.0	-0.0186(8)	-0.0170(5)	-0.0161(4)	-0.0153(3)	-0.0154(3)	-0.0166(3)
26.5	-0.0162(8)	-0.0160(5)	-0.0147(4)	-0.0146(3)	-0.0143(3)	-0.0146(3)
27.0	-0.0174(8)	-0.0142(5)	-0.0137(4)	-0.0133(3)	-0.0136(3)	-0.0139(3)
27.5	-0.0138(8)	-0.0134(5)	-0.0125(4)	-0.0123(3)	-0.0122(3)	-0.0127(3)
28.0	-0.0098(8)	-0.0102(5)	-0.0090(4)	-0.0095(3)	-0.0104(3)	-0.0102(3)
28.5	-0.0084(8)	-0.0081(5)	-0.0067(4)	-0.0071(3)	-0.0079(3)	-0.0083(3)
29.0	-0.0074(8)	-0.0052(5)	-0.0053(4)	-0.0055(3)	-0.0052(3)	-0.0064(3)
29.5	-0.0015(8)	-0.0028(5)	-0.0025(4)	-0.0027(3)	-0.0030(3)	-0.0033(3)
30.0	0.0009(8)	-0.0002(5)	-0.0000(4)	0.0006(3)	-0.0011(3)	-0.0013(3)
30.5	0.0045(8)	0.0030(5)	0.0032(4)	0.0014(3)	0.0016(3)	0.0014(3)
31.0	0.0078(8)	0.0050(5)	0.0040(4)	0.0056(4)	0.0039(3)	0.0038(3)
31.5	0.0093(8)	0.0071(5)	0.0065(4)	0.0061(3)	0.0062(3)	0.0056(3)
32.0	0.0122(8)	0.0086(5)	0.0078(4)	0.0085(3)	0.0079(3)	0.0069(3)
32.5	0.0123(8)	0.0108(5)	0.0091(4)	0.0098(3)	0.0095(3)	0.0095(3)
33.0	0.0133(8)	0.0115(5)	0.0096(4)	0.0108(3)	0.0098(3)	0.0096(3)
33.5	0.0141(8)	0.0108(5)	0.0102(4)	0.0113(3)	0.0108(3)	0.0108(3)
34.0	0.0119(8)	0.0120(5)	0.0101(4)	0.0112(4)	0.0099(3)	0.0105(3)
34.5	0.0136(9)	0.0114(5)	0.0092(4)	0.0102(3)	0.0104(3)	0.0107(3)
35.0	0.0120(8)	0.0109(5)	0.0091(4)	0.0096(3)	0.0100(3)	0.0090(3)

TABLE I. (*Continued*).

κ (nm^{-1})	I	II	III	IV	V	VI
35.5	0.0114(8)	0.0096(5)	0.0079(4)	0.0091(3)	0.0083(3)	0.0083(3)
36.0	0.0099(8)	0.0078(5)	0.0061(4)	0.0068(3)	0.0066(3)	0.0071(3)
36.5	0.0075(8)	0.0065(5)	0.0053(4)	0.0057(3)	0.0052(3)	0.0060(3)
37.0	0.0056(8)	0.0040(5)	0.0045(4)	0.0048(3)	0.0046(3)	0.0048(3)
37.5	0.0029(8)	0.0036(5)	0.0022(4)	0.0026(3)	0.0020(3)	0.0026(3)
38.0	0.0016(9)	0.0012(5)	0.0011(4)	0.0009(3)	0.0010(3)	0.0015(3)
38.5	0.0007(8)	-0.0007(5)	0.0000(4)	-0.0002(3)	-0.0005(3)	0.0000(3)
39.0	-0.0026(8)	-0.0008(5)	-0.0022(4)	-0.0009(3)	-0.0012(3)	-0.0008(3)
39.5	-0.0033(8)	-0.0025(5)	-0.0038(4)	-0.0028(3)	-0.0028(3)	-0.0031(3)
40.0	-0.0054(8)	-0.0028(5)	-0.0040(4)	-0.0035(3)	-0.0034(3)	-0.0045(3)
40.5	-0.0050(8)	-0.0039(5)	-0.0055(4)	-0.0046(3)	-0.0044(3)	-0.0042(3)
41.0	-0.0070(8)	-0.0050(5)	-0.0047(4)	-0.0050(3)	-0.0051(3)	-0.0054(3)
41.5	-0.0061(8)	-0.0042(5)	-0.0049(4)	-0.0054(3)	-0.0051(3)	-0.0055(3)
42.0	-0.0084(8)	-0.0058(5)	-0.0053(4)	-0.0054(3)	-0.0052(3)	-0.0057(3)
42.5	-0.0054(8)	-0.0056(5)	-0.0053(4)	-0.0044(3)	-0.0055(3)	-0.0056(3)
43.0	-0.0049(8)	-0.0048(5)	-0.0048(4)	-0.0046(3)	-0.0053(3)	-0.0052(3)
43.5	-0.0047(8)	-0.0043(5)	-0.0034(4)	-0.0037(3)	-0.0042(3)	-0.0047(3)
44.0	-0.0044(8)	-0.0048(5)	-0.0037(4)	-0.0040(3)	-0.0039(3)	-0.0044(3)
44.5	-0.0017(8)	-0.0033(5)	-0.0034(4)	-0.0032(3)	-0.0034(3)	-0.0032(3)
45.0	-0.0027(8)	-0.0026(5)	-0.0025(4)	-0.0025(3)	-0.0020(3)	-0.0026(3)
45.5	-0.0048(8)	-0.0021(5)	-0.0021(4)	-0.0019(3)	-0.0020(3)	-0.0023(3)
46.0	-0.0008(8)	0.0000(5)	-0.0010(4)	-0.0003(3)	-0.0007(3)	-0.0011(3)
46.5	-0.0012(8)	-0.0002(5)	-0.0009(4)	-0.0005(3)	-0.0002(3)	-0.0006(3)
47.0	0.0012(8)	-0.0004(5)	0.0009(4)	-0.0002(3)	0.0004(3)	0.0002(3)
47.5	0.0018(8)	0.0013(5)	0.0004(4)	0.0008(3)	0.0011(3)	0.0005(3)
48.0	0.0045(8)	0.0011(5)	0.0023(4)	0.0020(3)	0.0024(3)	0.0020(3)
48.5	0.0018(8)	0.0017(5)	0.0018(4)	0.0027(3)	0.0021(3)	0.0024(3)
49.0	0.0026(8)	0.0018(5)	0.0024(4)	0.0032(3)	0.0030(3)	0.0030(3)
49.5	0.0032(8)	0.0027(5)	0.0028(4)	0.0027(3)	0.0032(3)	0.0029(3)
50.0	0.0027(8)	0.0043(5)	0.0016(4)	0.0034(3)	0.0036(3)	0.0036(3)
50.5	0.0045(8)	0.0042(5)	0.0028(4)	0.0036(3)	0.0033(3)	0.0034(3)
51.0	0.0030(8)	0.0019(5)	0.0034(4)	0.0030(3)	0.0028(3)	0.0032(3)
51.5	0.0002(8)	0.0023(5)	0.0026(4)	0.0031(3)	0.0025(3)	0.0024(3)
52.0	0.0045(8)	0.0036(5)	0.0023(4)	0.0030(3)	0.0034(3)	0.0024(3)
52.5	-0.0004(8)	0.0028(5)	0.0016(4)	0.0021(3)	0.0019(3)	0.0024(3)
53.0	0.0008(8)	0.0013(5)	0.0020(4)	0.0014(3)	0.0011(3)	0.0023(3)
53.5	0.0021(8)	0.0016(5)	0.0016(4)	0.0012(3)	0.0008(3)	0.0010(3)
54.0	0.0039(8)	0.0017(5)	0.0015(4)	0.0007(3)	0.0010(3)	0.0009(3)
54.5	0.0013(8)	0.0010(5)	0.0011(4)	0.0006(3)	0.0004(3)	0.0004(3)
55.0	0.0003(8)	0.0011(5)	0.0003(4)	-0.0008(3)	0.0002(3)	0.0004(3)
55.5	-0.0007(8)	-0.0000(5)	-0.0002(4)	-0.0006(3)	-0.0002(3)	-0.0005(3)
56.0	-0.0008(8)	-0.0006(5)	-0.0006(4)	-0.0006(3)	-0.0008(3)	-0.0005(3)
56.5	0.0002(8)	-0.0013(5)	-0.0006(4)	-0.0004(3)	-0.0010(3)	-0.0012(3)
57.0	-0.0023(8)	-0.0025(5)	-0.0012(4)	-0.0019(3)	-0.0014(3)	-0.0009(3)
57.5	-0.0019(8)	-0.0026(5)	-0.0014(4)	-0.0017(3)	-0.0015(3)	-0.0017(3)
58.0	-0.0019(8)	-0.0012(5)	-0.0018(4)	-0.0023(3)	-0.0021(3)	-0.0015(3)
58.5	-0.0036(8)	-0.0025(5)	-0.0012(4)	-0.0024(3)	-0.0020(3)	-0.0020(3)
59.0	-0.0011(8)	-0.0021(5)	-0.0016(4)	-0.0018(3)	-0.0020(3)	-0.0018(3)
59.5	-0.0018(8)	-0.0022(5)	-0.0019(4)	-0.0015(3)	-0.0016(3)	-0.0021(3)
60.0	-0.0020(8)	-0.0018(5)	-0.0027(4)	-0.0013(3)	-0.0017(3)	-0.0022(3)
60.5	-0.0024(8)	-0.0019(5)	-0.0014(4)	-0.0024(3)	-0.0016(3)	-0.0018(3)
61.0	-0.0010(8)	-0.0009(5)	-0.0018(4)	-0.0017(3)	-0.0011(3)	-0.0016(3)
61.5	0.0003(8)	-0.0008(5)	-0.0014(4)	-0.0009(3)	-0.0009(3)	-0.0007(3)
62.0	-0.0003(8)	-0.0007(5)	-0.0008(4)	-0.0007(3)	-0.0006(3)	-0.0003(3)
62.5	-0.0013(8)	-0.0017(5)	-0.0009(4)	-0.0002(3)	-0.0004(3)	-0.0002(3)
63.0	0.0008(8)	-0.0002(5)	-0.0007(4)	0.0001(3)	-0.0008(3)	0.0000(3)
63.5	-0.0008(8)	0.0007(5)	0.0002(4)	0.0004(3)	0.0003(3)	-0.0000(3)
64.0	-0.0008(8)	-0.0006(5)	-0.0001(4)	0.0003(3)	0.0007(3)	0.0002(3)
64.5	-0.0003(8)	0.0008(5)	0.0009(4)	0.0011(3)	0.0011(3)	0.0006(3)
65.0	0.0013(8)	0.0006(5)	0.0010(4)	0.0011(3)	0.0006(3)	0.0011(3)
65.5	0.0014(8)	0.0002(5)	0.0012(4)	0.0015(3)	0.0014(3)	0.0015(3)
66.0	0.0007(8)	0.0010(5)	0.0016(4)	0.0009(3)	0.0012(3)	0.0010(3)
66.5	-0.0002(8)	0.0009(5)	0.0012(4)	0.0011(3)	0.0011(3)	0.0012(3)
67.0	0.0012(8)	0.0007(5)	0.0004(4)	0.0015(3)	0.0011(3)	0.0012(3)
67.5	0.0025(9)	0.0012(5)	0.0012(4)	0.0021(3)	0.0008(3)	0.0015(3)

TABLE I. (*Continued*).

κ (nm^{-1})	I	II	III	IV	V	VI
68.0	0.0021(8)	0.0015(5)	0.0020(4)	0.0013(3)	0.0009(3)	0.0010(3)
68.5	0.0024(8)	0.0017(5)	0.0010(4)	0.0011(3)	0.0014(3)	0.0017(3)
69.0	-0.0007(8)	0.0010(5)	-0.0001(4)	0.0009(3)	0.0007(3)	0.0005(3)
69.5	0.0016(8)	0.0009(5)	0.0013(4)	0.0009(3)	0.0005(3)	0.0013(3)
70.0	0.0026(8)	0.0014(5)	0.0021(4)	0.0013(3)	0.0010(3)	0.0012(3)
70.5	0.0004(8)	0.0012(5)	0.0013(4)	0.0002(3)	0.0004(3)	0.0006(3)
71.0	0.0012(8)	0.0002(5)	0.0006(4)	0.0007(3)	0.0001(3)	0.0005(3)
71.5	-0.0004(8)	-0.0006(5)	0.0005(4)	-0.0004(3)	0.0004(3)	-0.0001(3)
72.0	-0.0004(8)	-0.0004(5)	-0.0000(4)	0.0004(3)	0.0000(3)	-0.0005(3)
72.5	-0.0002(8)	0.0004(5)	0.0000(4)	0.0003(3)	-0.0006(3)	-0.0002(3)
73.0	0.0005(8)	0.0005(5)	0.0004(4)	0.0002(3)	-0.0003(3)	-0.0006(3)
73.5	0.0008(8)	0.0007(5)	0.0001(4)	-0.0006(3)	-0.0002(3)	-0.0006(3)
74.0	-0.0015(8)	-0.0002(5)	-0.0005(4)	-0.0010(3)	-0.0004(3)	0.0000(3)
74.5	-0.0011(8)	-0.0005(5)	-0.0011(4)	-0.0004(3)	-0.0004(3)	-0.0013(3)
75.0	-0.0013(8)	-0.0002(5)	-0.0004(4)	-0.0012(3)	-0.0005(3)	-0.0008(3)
75.5	-0.0006(8)	-0.0026(5)	-0.0024(4)	-0.0014(3)	-0.0012(3)	-0.0006(3)
76.0	-0.0010(8)	-0.0013(5)	-0.0013(4)	-0.0008(3)	-0.0010(3)	-0.0014(3)
76.5	-0.0017(9)	-0.0012(5)	-0.0011(4)	-0.0012(3)	-0.0007(3)	-0.0007(3)
77.0	-0.0002(8)	0.0001(5)	-0.0003(4)	-0.0010(3)	-0.0007(3)	-0.0011(3)
77.5	0.0006(8)	0.0009(5)	-0.0006(4)	0.0002(3)	-0.0009(3)	-0.0006(3)
78.0	-0.0008(8)	-0.0000(5)	-0.0012(4)	-0.0000(3)	-0.0001(3)	-0.0004(3)
78.5	-0.0014(8)	-0.0005(5)	-0.0012(4)	-0.0005(3)	-0.0006(3)	-0.0008(3)
79.0	0.0010(9)	-0.0004(5)	-0.0008(4)	-0.0009(3)	-0.0008(3)	-0.0007(3)
79.5	-0.0006(8)	0.0003(5)	0.0003(4)	0.0001(3)	0.0000(3)	-0.0009(3)
80.0	-0.0010(8)	-0.0005(5)	-0.0002(4)	-0.0001(3)	-0.0007(3)	-0.0001(3)
80.5	-0.0005(8)	0.0007(5)	0.0001(4)	-0.0004(3)	0.0003(3)	-0.0001(3)
81.0	0.0005(8)	0.0003(5)	0.0004(4)	-0.0003(3)	0.0002(3)	0.0003(3)
81.5	0.0011(8)	0.0004(5)	0.0003(4)	0.0000(3)	0.0000(3)	0.0001(3)
82.0	-0.0006(8)	0.0002(5)	0.0000(4)	0.0005(3)	-0.0000(3)	-0.0002(3)
82.5	0.0006(9)	-0.0003(5)	-0.0002(4)	-0.0001(3)	0.0005(3)	0.0007(3)
83.0	-0.0007(8)	0.0007(5)	0.0001(4)	0.0001(3)	0.0005(3)	0.0002(3)
83.5	-0.0017(8)	0.0007(5)	0.0007(4)	0.0002(3)	0.0006(3)	0.0006(3)
84.0	0.0010(9)	0.0009(5)	0.0006(4)	-0.0003(3)	0.0007(3)	0.0004(3)
84.5	0.0003(8)	-0.0001(5)	-0.0000(4)	0.0003(3)	0.0005(3)	0.0005(3)
85.0	-0.0009(8)	0.0006(5)	0.0007(4)	0.0004(3)	0.0007(3)	0.0003(3)
85.5	-0.0010(8)	-0.0004(5)	-0.0001(4)	0.0002(3)	0.0005(3)	-0.0002(3)
86.0	0.0021(8)	0.0005(5)	-0.0001(4)	0.0006(3)	0.0008(3)	0.0008(3)
86.5	0.0012(8)	0.0004(5)	0.0009(4)	0.0004(3)	0.0004(3)	0.0008(3)
87.0	0.0001(8)	-0.0006(5)	-0.0000(4)	-0.0001(3)	-0.0006(3)	-0.0003(3)
87.5	0.0005(8)	-0.0006(5)	0.0004(4)	0.0001(3)	0.0002(3)	-0.0001(3)
88.0	0.0007(8)	-0.0003(5)	0.0005(4)	0.0006(3)	-0.0001(3)	0.0006(3)
88.5	0.0013(9)	-0.0003(5)	-0.0001(4)	-0.0003(3)	0.0002(3)	0.0003(3)
89.0	-0.0010(8)	-0.0006(5)	0.0005(4)	0.0001(3)	0.0002(3)	0.0005(3)
89.5	0.0004(8)	-0.0008(5)	0.0002(4)	-0.0002(3)	-0.0005(3)	0.0002(3)
90.0	-0.0030(8)	-0.0007(5)	-0.0004(4)	0.0001(3)	-0.0001(3)	0.0003(3)
90.5	0.0004(8)	-0.0000(5)	-0.0004(4)	-0.0003(3)	-0.0003(3)	-0.0002(3)
91.0	0.0007(8)	-0.0001(5)	0.0002(4)	-0.0004(3)	-0.0003(3)	0.0004(3)
91.5	0.0006(8)	0.0003(5)	-0.0011(4)	-0.0004(3)	-0.0003(3)	-0.0006(3)
92.0	-0.0009(8)	-0.0011(5)	-0.0001(4)	-0.0005(3)	-0.0006(3)	-0.0001(3)
92.5	0.0002(8)	-0.0003(5)	0.0001(4)	-0.0002(3)	0.0001(3)	0.0000(3)
93.0	-0.0008(9)	-0.0008(5)	-0.0006(4)	-0.0002(3)	-0.0005(3)	-0.0006(3)
93.5	-0.0005(8)	-0.0007(5)	0.0002(4)	-0.0002(3)	-0.0004(3)	0.0001(3)
94.0	-0.0014(8)	-0.0006(5)	-0.0007(4)	-0.0004(3)	-0.0005(3)	-0.0003(3)
94.5	-0.0006(8)	0.0012(5)	0.0000(4)	0.0002(3)	0.0000(3)	-0.0001(3)
95.0	0.0002(8)	-0.0004(5)	-0.0005(4)	-0.0001(3)	-0.0008(3)	-0.0004(3)
95.5	0.0004(8)	-0.0010(5)	-0.0009(4)	-0.0007(3)	-0.0002(3)	-0.0008(3)
96.0	-0.0001(9)	-0.0002(5)	-0.0005(4)	0.0001(3)	0.0003(3)	0.0006(3)
96.5	0.0010(9)	0.0001(5)	0.0002(4)	-0.0007(3)	-0.0001(3)	0.0004(3)
97.0	0.0000(9)	0.0002(5)	0.0002(4)	-0.0004(3)	-0.0001(3)	-0.0006(3)
97.5	0.0002(8)	-0.0005(5)	0.0006(4)	-0.0005(3)	0.0002(3)	0.0004(3)
98.0	-0.0000(8)	-0.0006(5)	-0.0004(4)	-0.0004(3)	0.0001(3)	-0.0000(3)
98.5	0.0003(8)	-0.0014(5)	-0.0001(4)	0.0001(3)	-0.0005(3)	-0.0001(3)
99.0	-0.0004(8)	-0.0009(5)	-0.0005(4)	0.0002(3)	0.0002(3)	-0.0005(3)
99.5	-0.0005(9)	0.0000(5)	-0.0010(4)	0.0007(3)	-0.0002(3)	0.0003(3)
100.0	0.0000(8)	0.0006(5)	0.0010(4)	0.0003(3)	0.0002(3)	0.0000(3)

$$I(\kappa)=I_\infty a(\kappa)\left[1+n\frac{\langle b\rangle^2}{\langle b^2\rangle}H(\kappa)\right], \quad (33)$$

where $a(\kappa)$ denotes a small residual distortion of the data. From a fit of the four-parameter Verlet model,[33]

$$\kappa H(\kappa)=A\exp(-\beta\kappa)\cos[\gamma(\kappa-\kappa_0)], \quad (34)$$

at the higher κ values ($43\leq\kappa\leq129$ nm^{-1}) the data were normalized and $a(\kappa)$ was determined for each thermodynamic state. For $\langle b\rangle^2/\langle b^2\rangle$ the value 0.916 was used. The weighted mean-square deviation between the fitted model and the experimental data points,

$$\Delta^2=\frac{1}{N}\sum_{n=1}^{N}\left[\frac{F(\kappa_n)-I(\kappa_n)}{\Delta_n}\right]^2, \quad (35)$$

with Δ_n the estimated statistical accuracy of each data point, for all six experiments was in the range $1.2<\Delta^2<1.4$.

VIII. RESULTS AND DISCUSSION

The experimental values of $H(\kappa)$ in the range $4.0<\kappa<100.0$ nm^{-1} in steps of 0.5 nm^{-1} are given in Table I. The accuracy of $H(\kappa)$ decreases with decreasing density because the experiment was designed to determine $S(\kappa)$ for each state with the same statistical accuracy.

TABLE II. Densities and $S(0)$ calculated from Theeuwes and Bearman.

	T (K)	p (MPa)	n (nm^{-3})	$S(0)$	$H(0)$ (nm^3)
I	220	6.66	4.89	7.54	1.34
II	220	7.33	7.08	8.19	1.02
III	220	7.86	8.26	4.41	0.47
IV	200	4.58	11.02	1.42	0.038
V	200	5.83	11.55	0.86	−0.012
VI	200	7.69	12.06	0.63	−0.031

The accuracy at lower κ values is less. At the lowest κ value (4 nm^{-1}) close to the incoming beam $H(\kappa)$ is unreliable. There the procedure to correct for the (very high) background fails.

$S(0)$ and $H(0)$ for each state, calculated from p-V-T data of Theeuwes and Bearman,[24] are given in Table II. Comparison of $H(0)$ and $H(\kappa)$ at the lower κ values, given in Table I, shows that a simple extrapolation of $H(\kappa)$ to $\kappa=0$ is not possible.

The $H(\kappa)$'s obtained in the gas phase, plotted in Figs. 4(c) and 4(d), show clearly a density dependence along the 220-K isotherm. Up to $\kappa\approx40$ nm^{-1} the oscillations of $H(\kappa)$ are more pronounced the lower the density. The κ value where $H(\kappa)$ changes sign on the ascending slope of the main peak shifts to the right. This shift is also observed in Figs. 4(c) and 4(d), where the $H(\kappa)$'s for

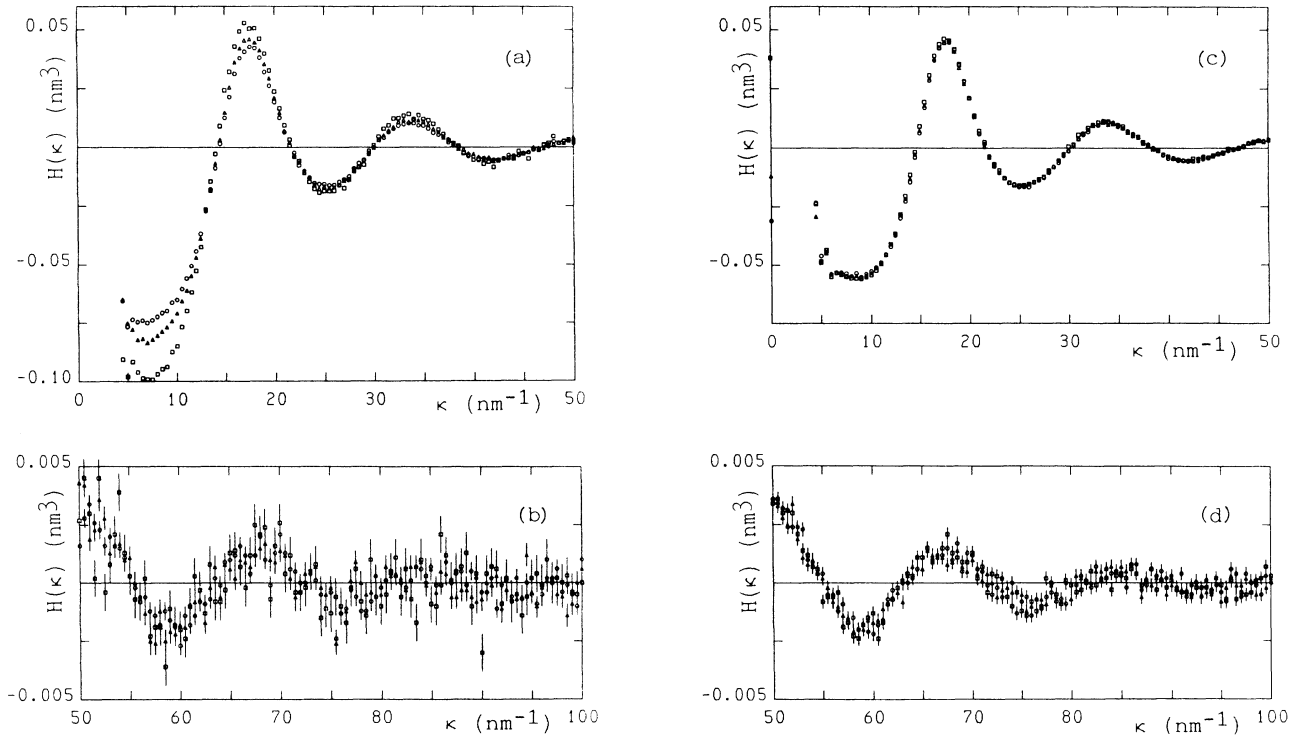

FIG. 4. (a) and (b) Experimental $H(\kappa)$'s for gaseous krypton at $T=220$ K [$n=4.89$, 7.08, and 8.26 nm^{-3} (squares, triangles, and circles)]; (c) and (d), the same for liquid krypton at $T=200$ K [$n=11.02$, 11.55, and 12.06 nm^{-3} (squares, triangles, and circles)].

the liquid phase at $T=200$ K are plotted. [$H(\kappa)$ changes sign in the liquid phase at larger κ than in the gas phase.] A further density dependence can hardly be observed on the scale of this plot. Therefore the isothermal density derivatives $\partial H(\kappa)/\partial n$ and $\partial^2 H(\kappa)/\partial n^2$ at the average density, shown in Figs. 5(a)–5(c) for the gas phase and in Figs. 5(d)–5(f) for the liquid phase, were estimated from finite differences. In the liquid phase the higher statistical accuracy of $H(\kappa)$ partly compensates for the smaller density range covered and $\partial H(\kappa)/\partial n$ has an accuracy of the same order as in the gas phase. The rightward shift of the rising slope of the main peak with increasing density is reflected in negative values of $\partial H(\kappa)/\partial n$ at the κ value where $H(\kappa)$ changes sign. For the gas phase $\partial H(\kappa)/\partial n$ and $H(\kappa)$ are approximately in antiphase and roughly proportional as follows from a "scatter plot" of $\partial H(\kappa)/\partial n$ versus $H(\kappa)$, shown in Fig. 6(a). In the liquid phase it is hardly possible to draw conclusions on $\partial H(\kappa)/\partial n$ beyond $\kappa=20$ nm^{-1} and a scatter plot of $\partial H(\kappa)/\partial n$ versus $H(\kappa)$ in the liquid phase given in Fig. 6(b) is less conclusive. Despite the lower accuracy, the data on $\partial^2 H(\kappa)/\partial n^2$ in the liquid phase seem to show some structure around the main peak, practically absent in the gas phase. In both cases the limited accuracy of the data prevents one from deriving conclusions from the second density derivative.

From $S(\kappa)$'s of gaseous krypton along the 218-K isotherm (estimated densities $n=3$ and 5 nm^{-3}) ". . . obtained graphically from smooth curves drawn through the experimental points" by Winfield and Egelstaff[34] $H(\kappa)$ and $\partial H(\kappa)/\partial n$, shown in Fig. 7, are derived. The structure in $H(\kappa)$ is more pronounced than in the present experiments in the gas phase at 220 K and higher densities [cf. Fig. 4(a)]. In the region of the main peak $\partial H(\kappa)/\partial n$ and $H(\kappa)$ are in antiphase and no shift of the rising slope with increasing density is observed. $H(\kappa)$ at $T=218$ K extrapolated linearly to $n=6.75$ nm^{-3}, agrees fairly well with the present data except at lower κ (cf. Fig. 8).

The "high"-density part ($n=3$–6 nm^{-3}) of data by Teitsma and Egelstaff[1] on gaseous krypton at $T=297$ K and densities between $n=0.2$ and 6.2 nm^{-3} was used to determine $H(\kappa)$ and $\partial H(\kappa)/\partial n$ shown in Figs. 9(a) and

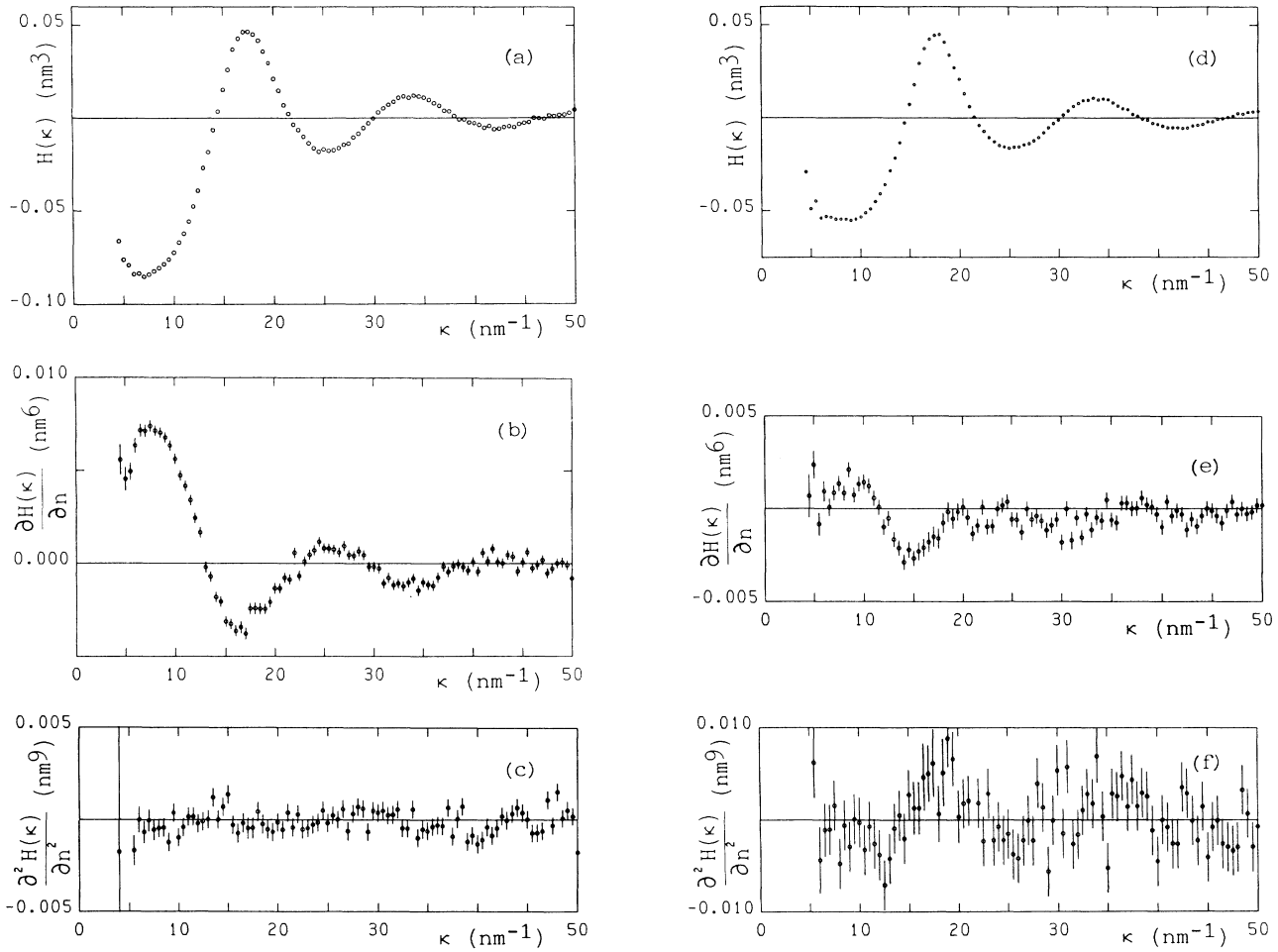

FIG. 5. (a)–(c) $H(\kappa)$, $\partial H(\kappa)/\partial n$, and $\partial^2 H(\kappa)/\partial n^2$ for gaseous krypton ($T=220$ K, $n=6.75$ nm^{-3}); (d)–(f) the same for liquid krypton ($T=200$ K, $n=11.55$ nm^{-3}).

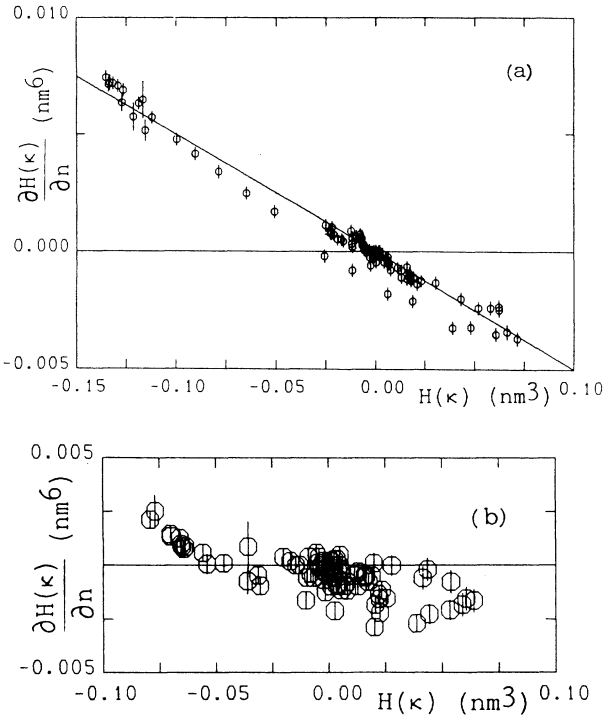

FIG. 6. (a) Scatter plot of $\partial H(\kappa)/\partial n$ vs $H(\kappa)$ for gaseous krypton at $T=220$ K [the line represents $\partial H(\kappa)/\partial n = -0.05H(\kappa)$]; (b) the same for liquid krypton at $T=200$ K.

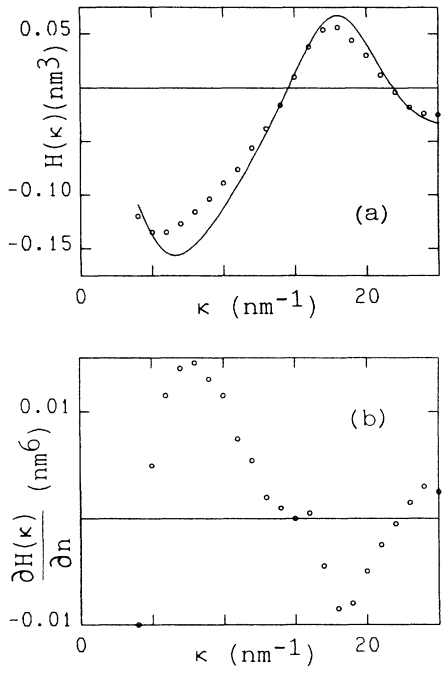

FIG. 7. (a) $H(\kappa)$ for gaseous krypton [$T=218$ K, $n=3$ and 5 nm^{-3} (line and circles)] from data of Winfield and Egelstaff (Ref. 34); (b) $\partial H(\kappa)/\partial n$ from these data.

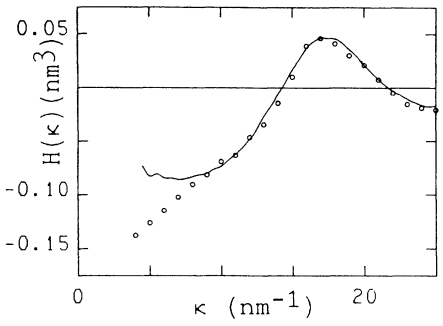

FIG. 8. $H(\kappa)$ for gaseous krypton at $n=6.75$ nm^{-3} from present experiments ($T=220$ K, line) and from extrapolation of data of Winfield and Egelstaff (Ref. 34) ($T=218$ K, circles).

9(b). $\partial H(\kappa)/\partial n$ from these data is surprisingly similar to the one in the liquid phase at $T=200$ K and higher density $n \approx 11.5$ nm^{-3} [cf. Fig. 5(e)].

$H(\kappa)$ and $\partial H(\kappa)/\partial n$, determined from structure-factor data on liquid neon at $T=35$ K and $n \approx 33.5$ nm^{-3} by De Graaf and Mozer[35] and for liquid argon at approximately corresponding states ($T=120$ K and $n \approx 19$ nm^{-3}) by Van

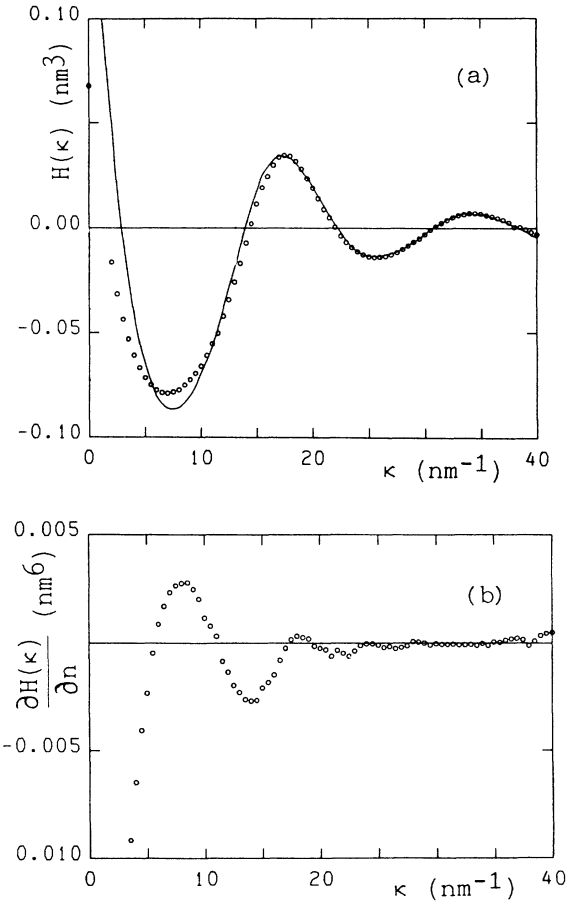

FIG. 9. (a) $H(\kappa)$ for gaseous krypton [$T=297$ K, $n=3.16$ and 6.19 nm^{-3} (line and circles)] from data of Teitsma and Egelstaff (Ref. 1); (b) $\partial H(\kappa)/\partial n$ from these data.

Well *et al.*,[36,37] are shown in Figs. 10(a) and 10(b) and Figs. 11(a) and 11(b). $\partial H(\kappa)/\partial n$'s from these data show a negative peak at the κ value where $H(\kappa)$ changes sign on the rising slope of the main peak, followed by a positive peak located at the second half of the main peak, absent in the krypton data.

Recently Aers and Dharma-wardana[6] successfully interpreted the structure-factor data on gaseous krypton at room temperature of Teitsma and Egelstaff,[1] using the Rosenfeld-Ashcroft MHNC approximation with the Barker two-body potential[3] and an effective (lowest-order) AT three-body potential.[5] For the present thermodynamic states MHNC calculations were performed in close collaboration with Dharma-wardana and Aers.

The thermodynamically consistent values of the packing fraction η that describes the bridge function in the MHNC calculations with the Barker potential (cf. Ref. 6) could excellently be represented by $\eta = an + bn^2$ with $a = 0.022\,558$ nm^3 and $b = 0.000\,260$ nm^6 for the liquid states at $T = 200$ K. (The reported linear dependence of this η on n at room temperature[6] should be replaced by a function with a significant quadratic contribution at higher densities.[20]) For gaseous krypton at $T = 220$ K the MHNC procedure failed to yield thermodynamically consistent values for η at the two lower densities. At the higher density $n = 8.26$ nm^{-3} the value $\eta = 0.200$ was obtained. Whether this failure is a peculiarity of the MHNC procedure or whether it reflects that the equation of state of the pair fluid may be different from the one of the real fluid (with a different coexistence region) is not clear at the moment.

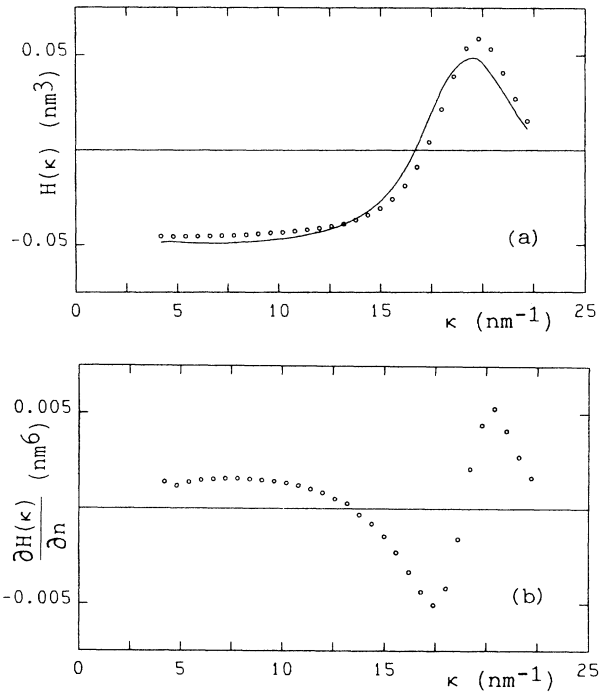

FIG. 11. (a) $H(\kappa)$ for liquid argon [$T = 120$ K, $n = 17.6$ and 20.7 nm^{-3} (line and circles)] from data of Van Well *et al.* (Refs. 36 and 37); (b) $\partial H(\kappa)/\partial n$ from these data.

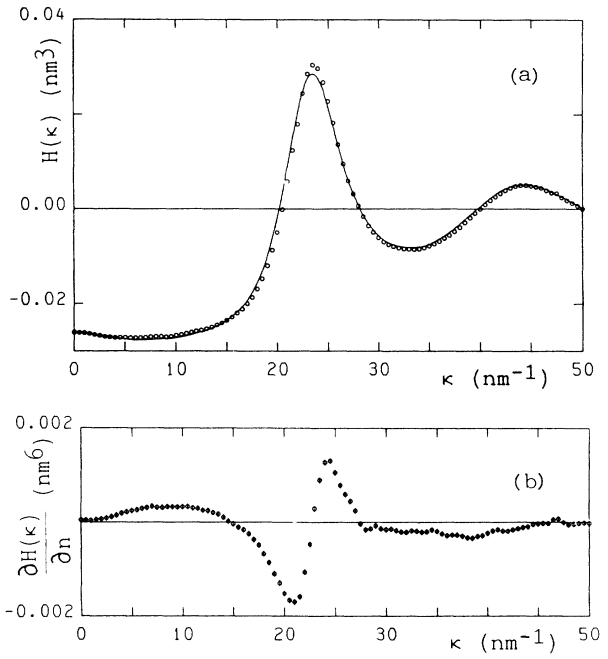

FIG. 10. (a) $H(\kappa)$ for liquid neon [$T = 35$ K, $n = 31.7$ and 34.7 nm^{-3} (line and circles)] from data of De Graaf and Mozer (Ref. 35); (b) $\partial H(\kappa)/\partial n$ from these data.

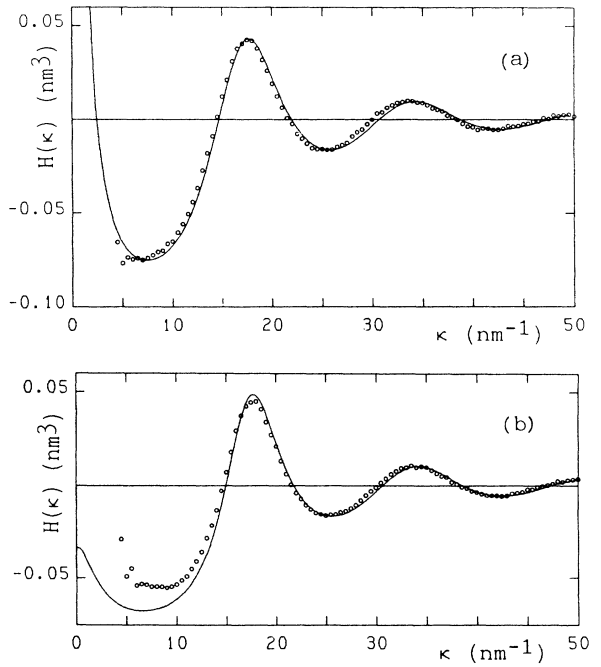

FIG. 12. (a) $H(\kappa)$ for gaseous krypton ($T = 220$ K, $n = 8.26$ nm^{-3}) from MHNC (line) and from present experiment (circles); (b) the same for liquid krypton ($T = 200$ K, $n = 11.5$ nm^{-3}).

Values of $H(\kappa)$ from MHNC calculations with the Aziz[4] pair potential were found to be practically identical to those obtained with the Barker[3] potential. Compared to the experimental data, $H(\kappa)$'s from the MHNC calculations with the Barker (or the Aziz) two-body potential are shifted slightly to the right. The shift is more pronounced at the rising slopes than at the descending slopes as can be observed from Fig. 12.

The introduction of an effective AT correction to the potential, fitted to the data with the constraint that $S(0)$ should be equal to the known "compressibility limit," hardly gave an improvement. Without this constraint the strength of the effective AT correction could be fitted to yield a better agreement with the data; however, in that case the value of $S(0)$ was far from the compressibility limit [cf. Figs. 13(a) and 13(b)]. In Fig. 13(c) $h(r)$ that corresponds with the latter case is shown together with the "experimental" $h(r)$, which is obtained using a nonconventional Fourier-transform procedure that diminishes effects due to truncation and statistical noise in $H(\kappa)$ (cf. Appendix B). The nonconsistent dependence of $S(\kappa=0)$ on the effective potential leads to the conclusion that interpretation of the data using the MHNC procedure with an effective AT correction is less successful than at room temperature.

Barocchi *et al.*[15] determined $H(\kappa)$'s from MD simulations with 500 atoms at the densities and temperatures of the present experiments using both the Barker pair potential for the interaction between the atoms, and this potential together with the AT three-body potential. In contrast to the MHNC calculations, no singularities were encountered at the two lower densities on the 220-K isotherm. The differences between corresponding MD data for the two systems turn out to be very small and in view of the (correlated) inaccuracies hardly significant. The observed differences are much smaller than might be expected from a first-order estimate in agreement with observations by Ram *et al.*[38] and Hoheisel.[39]

In Fig. 14(a) the experimental $H(\kappa)$ at $T=220$ K and $n=4.89$ nm^{-3} is shown together with the MD data and similarly in Fig. 14(b) for $T=200$ K and $n=12.06$ nm^{-3}. Compared to the experimental data the MD data are shifted slightly to the right, similar to the MHNC data. Within the accuracy of the experimental and the MD data the density dependence of the $H(\kappa)$'s is not significantly different. The negative peak in $\partial H(\kappa)/\partial n$ at the ascending slope of the main peak is also observed in the simulat-

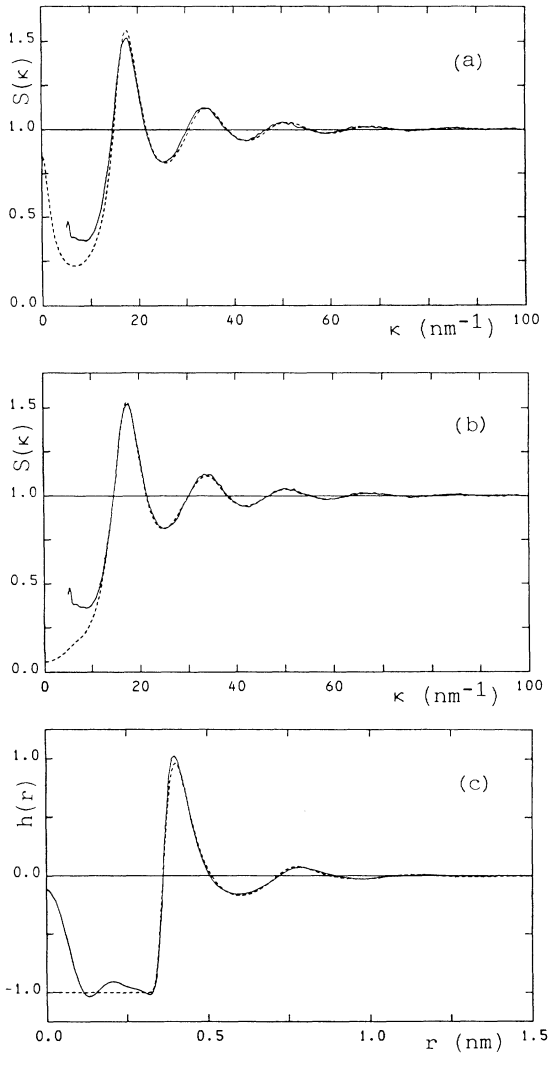

FIG. 13. (a) $S(\kappa)$ for liquid krypton ($T=200$ K, $n=11.5$ nm^{-3}) from experiment (line) and from MHNC with AT correction with $S(0)=0.86$ fixed; (b) the same with $S(0)$ free; (c) $h(r)$ from experiment (line) and from MHNC corresponding to (b) (dashed).

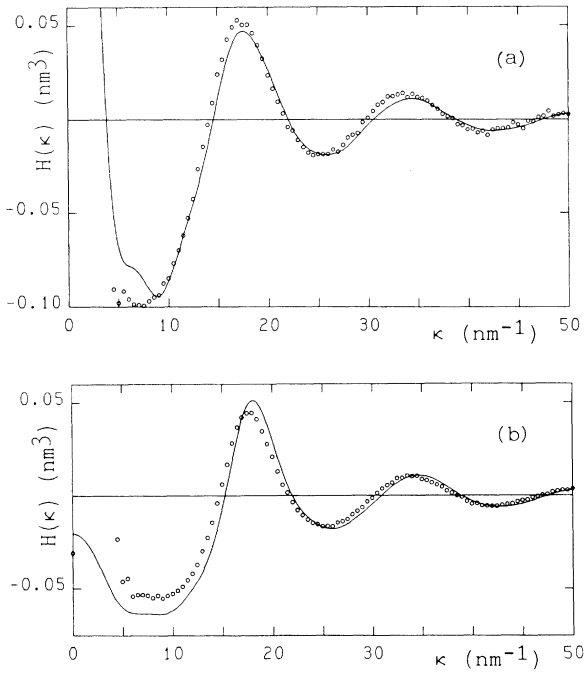

FIG. 14. (a) $H(\kappa)$ for gaseous krypton ($T=220$ K, $n=4.89$ nm^{-3}) from MD by Barocchi *et al.* (Ref. 15) (line) and from present experiment (circles); (b) the same for liquid krypton ($T=200$ K, $n=12.06$ nm^{-3}).

ed data. Unfortunately, the MD data are less decisive for $\partial H(\kappa)/\partial n$ at the second half of the main peak.

It is expected that similar results will be obtained using the Aziz[4] instead of the Barker[3] pair potential. Apart from the question whether or not the pair or pair + AT fluids correspond to the real fluid in the region of (although not close to) the critical point, the number of atoms in the simulated system might influence the results.

IX. CONCLUSIONS

The Fourier transform of the total correlation function $h(r)$, $H(\kappa)$, is obtained from accurate neutron diffraction data for krypton at three densities along a supercritical isotherm and at three densities along a subcritical isotherm in the liquid phase. Isothermal density derivatives of $H(\kappa)$ were determined at both temperatures. Compared to density derivatives for liquid argon and neon, determined from recent neutron scattering experiments, significant differences are observed in $\partial H(\kappa)/\partial n$ at the second half of the main diffraction peak. A surprising similarity is observed between $\partial H(\kappa)/\partial n$ in the liquid phase and $\partial H(\kappa)/\partial n$ determined from recent neutron-diffraction data on gaseous krypton at room temperature and low densities.

A comparison with modified-hypernetted-chain and molecular-dynamics calculations, using the Barker[3] pair potential with and without an (effective) Axilrod-Teller three-body potential, shows that, although a reasonable agreement is obtained, the present data differ significantly from the theoretical predictions (the same results are expected for the Aziz[4] pair potential). This suggests that the Axilrod-Teller three-body potential is inadequate to describe effectively the influence of more-body potentials on the structure of krypton at the thermodynamic states investigated here.

ACKNOWLEDGMENTS

It was a pleasure to collaborate with Chandre Dharma-wardana and Geof Aers on modified-hypernetted-chain calculations during a short visit (supported financially by the ERR fund of the Technische Universiteit Delft) to the National Research Council of Canada in Ottawa. I am obliged to Fabrizio Barocchi, Marco Zoppi, and Renato Magli of the University of Florence (Italy) for their molecular-dynamics calculations. Many discussions with Peter Verkerk and Jan van Tricht are gratefully acknowledged. I thank J. J. van Loef for his interest in this work.

APPENDIX A: STATISTICAL TESTS

In a preset monitor counting experiment the probability of observing d counts in the detector, while the monitor has counted its preset value m, is described by the negative binomial distribution

$$P_m(d)=\begin{pmatrix} d+m-1 \\ m-1 \end{pmatrix}\delta^d(1+\delta)^{-(m+d)} , \tag{A1}$$

with expectation

$$E(d)=m\delta=\lambda \tag{A2}$$

and variance

$$\Delta^2=E([d-m\delta]^2)=m\delta(1+\delta)=\lambda\left[1+\frac{\lambda}{m}\right] . \tag{A3}$$

Repeated measurements need to be averaged and normalized to a common preset monitor count m. The maximum-likelihood estimator (MLE) from N data point d_i with (different) monitor counts m_i,

$$I=m\frac{\sum_{i=1}^{N} d_i}{\sum_{i=1}^{N} m_i}, \quad E(I)=m\delta=\lambda , \tag{A4}$$

with variance

$$\Delta^2 I=\frac{m}{\sum_{i=1}^{N} m_i}m\delta(1+\delta)=\frac{m}{\sum_{i=1}^{N} m_i}\lambda\left[1+\frac{\lambda}{m}\right] , \tag{A5}$$

is used as the "average" normalized to m monitor counts. Unbiased estimates for the variance Eq. (A5) are given by

$$\Delta^2=\frac{m}{1+\sum_{i=1}^{N} m_i}I\left[1+\frac{I}{m}\right] , \tag{A6}$$

and

$$\Delta^2_{\text{exp}}=\frac{m^2}{\left[\sum_{i=1}^{N} m_i\right]^2-\sum_{i=1}^{N} m_i^2}\sum_{i=1}^{N}\left[d_i-\frac{m_i}{m}I\right]^2 . \tag{A7}$$

For $m_i=m$ Eq. (A4) and (A7) reduce to

$$\begin{aligned} I&=\frac{1}{N}\sum_{i=1}^{N} d_i , \\ \Delta^2&=\frac{m}{1+mN}I\left[1+\frac{I}{m}\right] , \\ \Delta^2_{\text{exp}}&=\frac{1}{N(N-1)}\sum_{i=1}^{N}(d_i-I)^2 . \end{aligned} \tag{A8}$$

The variance of Δ^2 is in general much smaller than the variance of Δ^2_{exp}; therefore, Δ^2 is used to estimate the variance of I.

Possible "outliers" can influence severely the average in Eq. (A4); therefore, a test should be done to detect and remove outliers. The median I_m of the individually normalized intensities $I_i=md_i/m_i$ is a more robust estimate for λ and is used in the test as follows. Only data points that satisfy

$$\begin{aligned} &I_m-2.56\Delta_i<I_i<I_m+2.56\Delta_i , \\ &\Delta_i^2=\frac{m}{m_i+1}I_m\left[1+\frac{I_m}{m}\right] , \end{aligned} \tag{A9}$$

are used for the normalized average Eq. (A4). Under nor-

mal conditions approximately 1% of the data is expected to be outside the interval given in Eq. (A9). If the fraction of rejected data is significantly larger an external source of noise must be present.

This procedure was applied on line to the ten submeasurements at each detector position. At a given instance the number of outliers in the on-line check increased to 20%. The time utilized for the measurements was effectively reduced to 80% because of duly rejected subresults during a short period until the external source of noise could be identified. It can be estimated that, without the procedure using subresults, the number of measurements not affected by the spurious noise would have been reduced to only 11%.

The same procedure as described above was applied off line on corresponding data points $I_i(\kappa)$ of repeated series. Moreover, for each series the sequence (as a function of κ) of the sign of the deviation of $I_i(\kappa)$ from $I(\kappa)$ was studied. In particular the number of positive and negative residues was determined. Then the number of runs, defined as a sequence of residues with equal sign, was determined for each series and compared with the expectation of the number of runs.[40] The number of residues is indicative for long-term effects while the runs check is indicative for short-term effects. No indications were found that any series, or significant parts thereof, should be rejected.

APPENDIX B: FOURIER TRANSFORMATION

To estimate $h(r)$ from the experimental data points $H(\kappa_i)$, at equidistant κ_i values with separation Δ, the integral (13) was separated into a low-κ range and a high-κ range,

$$h(r)=h^-(r)+h^+(r) ,$$

$$h^-(r)=\frac{1}{2\pi^2 r}\int_0^{\kappa_m}\kappa H(\kappa)\sin(\kappa r)d\kappa , \tag{B1}$$

$$h^+(r)=\frac{1}{2\pi^2 r}\int_{\kappa_m}^{\infty}\kappa H(\kappa)\sin(\kappa r)d\kappa .$$

For the estimate of $h^-(r)$ the function $\kappa H(\kappa)$ was represented by a weighted cubic spline function fitted to the data at low-κ values according to Reinsch[41] [in fact the spline fit was applied in the range $-\kappa_m<\kappa<\kappa_m$, with $H(-\kappa_i)$ defined equal to $H(\kappa_i)$ and $\kappa_m=55\ \mathrm{nm}^{-1}$],

$$\kappa H(\kappa)\approx A_i+B_i\alpha+C_i\alpha^2+D_i\alpha^3,\quad i=0,1,\ldots,N-1 , \tag{B2}$$

$$0<\alpha=\kappa-\kappa_i<\Delta ,$$

which can be transformed analytically with the result

$$h^-(r)\approx\frac{1}{2\pi^2 r}\sum_{n=1}^{4}\left[s_n(r)\sum_{i=0}^{N-1}x_i^n\sin(\kappa_i r)+c_n(r)\sum_{i=0}^{N-1}x_i^n\cos(\kappa_i r)\right] ,$$

$$x_i^{1,2,3,4}=A_i,B_i,C_i,D_i . \tag{B3}$$

The discrete sine and cosine transforms of the spline coefficients, $\sum_i x_i\sin\kappa_i r$ and $\sum_i x_i\cos\kappa_i r$, are conveniently evaluated using the FFT algorithm. The r-dependent coefficients $s_1(r),\ldots,s_4(r)$ and $c_1(r),\ldots,c_4(r)$ are given by

$$s_1(r)=\frac{1}{r}\sin(r\Delta) ,$$

$$s_2(r)=\frac{1}{r}\left[\frac{1}{r}[\cos(r\Delta)-1]+\Delta\sin(r\Delta)\right] ,$$

$$s_3(r)=\frac{1}{r}\left[-\frac{2}{r^2}\sin(r\Delta)+2\frac{\Delta}{r}\cos(r\Delta)+\Delta^2\sin(r\Delta)\right] ,$$

$$s_4(r)=\frac{1}{r}\left[\frac{6}{r^3}[1-\cos(r\Delta)]-6\frac{\Delta}{r^2}+3\frac{\Delta^2}{4}\cos(r\Delta)+\Delta^3\sin(r\Delta)\right] , \tag{B4}$$

$$c_1(r)=\frac{1}{r}[1-\cos(r\Delta)] ,$$

$$c_2(r)=\frac{1}{r}\left[\frac{1}{r}\sin(r\Delta)-\Delta\cos(r\Delta)\right] ,$$

$$c_3(r)=\frac{1}{r}\left[\frac{1}{r^2}[\cos(r\Delta)-1]+\frac{\Delta}{r}\sin(r\Delta)-\Delta^2\cos(r\Delta)\right] .$$

$$c_4(r)=\frac{1}{r}\left[\frac{1}{r^3}\sin(r\Delta)+\frac{\Delta}{r^2}\cos(r\Delta)+3\frac{\Delta^2}{r}\sin(r\Delta)-\Delta^3\cos(r\Delta)\right] .$$

Due to the cancellation of numerically calculated terms in $s_n(r)$ and $c_n(r)$ spurious results may be obtained in the case where $r\ll 1/\Delta$. Therefore the functions $s_1(r),\ldots,c_4(r)$ should be replaced for $r<1/\Delta$ by their rapidly converging Taylor series

$$s_n(r)=\Delta^n\sum_{i=0}^{\infty}(-1)^i(r\Delta)^{2i}/[(2i)!(2i+n)] ,$$

$$c_n(r)=r\Delta^{n+1}\sum_{i=0}^{\infty}(-1)^i(r\Delta)^{2i}/[(2i+1)!(2i+n+1)] . \tag{B5}$$

For the estimate of $h^+(r)$ the function $\kappa H(\kappa)$ was represented by the Verlet model[33] fitted to the data at high-κ values,

$$\kappa H(\kappa)=A\exp(-\beta\kappa)\cos[\gamma(\kappa-\kappa_0)],\quad \kappa_m\geq\kappa \tag{B6}$$

which can be evaluated analytically with the result

$$h^+(r)=\frac{A}{4\pi^2 r}\exp(-\beta\kappa_m)[F(r,\gamma)+F(r,-\gamma)]\ , \tag{B7}$$

$$F(r,\gamma)=\frac{\beta\sin[(r+\gamma)\kappa_m-\gamma\kappa_0]+(r+\gamma)\cos[(r+\gamma)\kappa_m-\gamma\kappa_0]}{(r+\gamma)^2+\beta^2}\ . \tag{B8}$$

It may be expected that termination errors and the influence of statistical inaccuracies in the data are diminished by this procedure. However, as the models do not describe the data exactly, systematic errors may be introduced in the transforms.

[1]A. Teitsma and P. A. Egelstaff, Phys. Rev. A **21**, 367 (1980).

[2]P. A. Egelstaff, A. Teitsma, and S. S. Wang, Phys. Rev. A **22**, 1702 (1980).

[3]J. A. Barker, R. O. Watts, J. K. Lee, T. P. Schafer, and Y. T. Lee, J. Chem. Phys. **61**, 3081 (1974).

[4]R. A. Aziz and M. J. Slaman, Mol. Phys. **58**, 679 (1986).

[5]B. M. Axilrod and E. Teller, J. Chem. Phys. **11**, 299 (1943).

[6]G. C. Aers and M. W. C. Dharma-wardana, Phys. Rev. A **29**, 2734 (1984).

[7]W. Schommers, Phys. Rev. A **22**, 2855 (1980).

[8]J. A. Barker, Phys. Rev. Lett. **57**, 230 (1986).

[9]P. A. Egelstaff (unpublished).

[10]P. A. Egelstaff, W. Glaser, D. Litchinsky, E. Schneider, and J.-B. Suck, Phys. Rev. A **27**, 1106 (1983).

[11]S. Yip, W. Alley, and B. Alder, J. Stat. Phys. **27**, 2101 (1982).

[12]P. A. Egelstaff, J. J. Salacuse, W. Schommers, and J. Ram, Phys. Rev. A **30**, 374 (1984).

[13]J. J. Salacuse, W. Schommers, and P. A. Egelstaff, Phys. Rev. A **34**, 1516 (1986).

[14]H. Fredrikze, Mol. Phys. **48**, 903 (1983).

[15]F. Barocchi, M. Zoppi, and R. Magli (private communication).

[16]W. Marshall and S. W. Lovesey, *Theory of Thermal Neutron Scattering* (Clarendon, Oxford, 1971).

[17]G. E. Bacon, *Neutron Diffraction* (Clarendon Press, Oxford, 1962).

[18]J. L. Yarnell, M. J. Katz, R. G. Wenzel, and S. H. Koenig, Phys. Rev. A **7**, 2130 (1973).

[19]G. E. Uhlenbeck, *Statistical Physics* (W. A. Benjamin, New York, 1963).

[20]H. Fredrikze, Ph.D. Thesis, Technical University Delft (1985).

[21]F. Zernike and J. A. Prins, Z. Phys. **41**, 184 (1927).

[22]It took Zernike and Prins in 1926 quite some time before they dared to replace $g_2(\mathbf{r},\mathbf{r}')$ in Eq. (9) by $h(r)$ to obtain Eq. (11), J. A. Prins [on the occasion of the M.Sc. examination of J. J. van Lieshout (unpublished) (1969)]; J. B. van Tricht (private communication).

[23]H. Fredrikze and J. B. van Tricht, Proceedings of the Conference on New Methods in Neutron Diffraction, Reactor Centrum Nederland, Report No. RCN-234, 1975 (unpublished).

[24]F. Theeuwes and R. J. Bearman, J. Chem. Thermodyn. **2**, 17 (1970).

[25]G. H. Vineyard, Phys. Rev. **91**, 239 (1954).

[26]J. R. D. Copley, Comput. Phys. Commun. **7**, 289 (1974).

[27]J. R. D. Copley, Comput. Phys. Commun. **20**, 459 (1980).

[28]J. R. D. Copley, Comput. Phys. Commun. **21**, 431 (1981).

[29]J. R. D. Copley, P. Verkerk, A. A. van Well, and H. Fredrikze, Comput. Phys. Commun. **40**, 337 (1986).

[30]F. Boutron and P. Mériel, Bull. Soc. Fr. Minér. Crist. **83**, 125 (1960).

[31]V. F. Sears, Atomic Energy of Canada Limited, Report No. AECL-8176, 1983 (unpublished).

[32]V. F. Sears, J. Appl. Cryst. **17**, 226 (1984).

[33]L. Verlet, Phys. Rev. **165**, 201 (1968).

[34]D. J. Winfield and P. A. Egelstaff, Can. J. Phys. **51**, 1965 (1973).

[35]L. A. de Graaf and B. Mozer, J. Chem. Phys. **55**, 4967 (1971).

[36]A. A. van Well, P. Verkerk, L. A. de Graaf, J.-B. Suck, and J. R. D. Copley, Phys. Rev. A **31**, 3391 (1985).

[37]A. A. van Well, P. Verkerk, and L. A. de Graaf, Interuniversitair Reactor Instituut (Delft) Report No. IRI-132-82-07/1, 1984 (unpublished).

[38]J. Ram and P. A. Egelstaff, Phys. Chem. Liq. **14**, 29 (1984).

[39]C. Hoheisel, Phys. Rev. A **23**, 1998 (1981).

[40]J. B. van Tricht, Interuniversitair Reactor Instituut (Delft), Report No. IRI-132-74-05, 1974 (unpublished).

[41]C. H. Reinsch, Numer. Math. **10**, 177 (1967).